

Effect of an imaginary part of the Schwinger-Dyson equation at finite temperature and density

S. Sasagawa and H. Tanaka

Department of Physics, Rikkyo University, Tokyo 171-8501, Japan

(Received 19 December 2011; revised manuscript received 9 February 2012; published 4 April 2012)

We examined the effect of an imaginary part of the ladder approximation Schwinger-Dyson equation. We show that the imaginary part enhances the effect of the first-order transition and affects a tricritical point. In particular, a chemical potential at the tricritical point is displaced about 200 MeV. Thus, one should not ignore the imaginary part. However, because the imaginary part is small away from the tricritical point, one should be able to ignore the imaginary part. In addition, we also examined the contribution of the wave-function renormalization constant.

DOI: [10.1103/PhysRevC.85.045201](https://doi.org/10.1103/PhysRevC.85.045201)

PACS number(s): 12.38.Lg, 11.30.Rd, 11.10.Wx, 24.85.+p

I. INTRODUCTION

Chiral symmetry breaking is restored at high temperature and density. Chiral symmetry breaking and restoration at zero and finite temperature are extensively studied by lattice QCD simulation. Quark-gluon plasma at high temperature has been observed at the BNL Relativistic Heavy Ion Collider (RHIC) [1]. On the other hand, there is an incomplete understanding of phenomena at low temperature and high density. Although it is expected that various phases exist in the region of low temperature and high density [2], we do not have sufficient information. For example, the lattice QCD at low temperature and high density is still inadequate by the sign problem. (This problem arises from the fermion determinant that is complex. Several methods for the sign problem have been developed; see, e.g., Refs. [3–5].) Furthermore, in addition to incomplete lattice simulation, there is little information from experimental data. Thus, it is very important to investigate this region.

The Schwinger-Dyson equation (SDE) is a useful tool at nonzero temperature and chemical potential [6–10]. This method can be used at low temperature and high density. For example, the SDE with the hard dense loop approximation can give the mass gap for color superconductivity [10]. For chiral symmetry breaking and restoration, the SDE shows that the phase transition is of second order at finite temperature and is of first order at nonzero chemical potential [6,7,9]. This has been shown in the context of models for spontaneously broken chiral symmetry (other than QCD), i.e., the Nambu-Jona-Lasinio model [11]. Moreover, several models show the existence of a tricritical point [12].

The SDE at nonzero chemical potential has an imaginary part. Because the imaginary part is generated by the presence of a chemical potential, the imaginary part has the effect of a chemical potential. This has been studied in Ref. [9], and it was shown that the effect is strong.

Because the approximate form for the exact quark propagator was used in Ref. [9], we verify the effect of the imaginary part using the more general form for the exact quark propagator at nonzero temperature and chemical potential. (We do not consider the Debye screening and the two-flavor superconductivity.) The more general quark propagator at nonzero temperature and chemical potential is the SO(3) invariant form and has the wave-function renormalization constant. We also study this effect for a tricritical point.

The paper is organized as follows. In Secs. II and III, we review the formulation at nonzero temperature and chemical potential. We show numerical results by solving the SDE in Sec. IV, and a summary is found in Sec. V.

II. FORMULATION AT NONZERO TEMPERATURE AND CHEMICAL POTENTIAL

We use the imaginary time formalism to analyze a phase transition at nonzero temperature and chemical potential [13, 14]. The ensemble average of an operator at temperature $T = 1/\beta$ and chemical potential μ is defined as

$$\langle \hat{O} \rangle_\beta = Z^{-1} \text{tr}[e^{-\beta(\hat{H} - \mu \hat{Q})} \hat{O}], \quad Z = \text{tr}[e^{-\beta(\hat{H} - \mu \hat{Q})}], \quad (1)$$

where \hat{H} and \hat{Q} are a Hamiltonian and a number operator. The partition function Z for bosons can be rewritten by

$$Z = \int \mathcal{D}\phi \mathcal{D}\phi^* \int \mathcal{D}\pi \mathcal{D}\pi^* \exp \left[\int_0^\beta d\tau \int d^3x \times \left(i\pi \frac{\partial \phi}{\partial \tau} + i\pi^* \frac{\partial \phi^*}{\partial \tau} - \mathcal{H}(\pi, \pi^*, \phi, \phi^*) + \mu Q \right) \right], \quad (2)$$

where τ is imaginary time $\tau = it$, $0 \leq \tau \leq \beta$. The field $\phi(\tau, \mathbf{x})$ has the periodicity $\phi(0, \mathbf{x}) = \phi(\beta, \mathbf{x})$. When the Lagrangian of the complex scalar field is used, the partition function is

$$Z = N(\beta) \int \mathcal{D}\phi \mathcal{D}\phi^* \exp \left[\int_0^\beta d\tau \int d^3x \mathcal{L} \right], \quad (3)$$

with

$$\mathcal{L} = - \left(\frac{\partial \phi}{\partial \tau} - \mu \phi \right) \left(\frac{\partial \phi^*}{\partial \tau} + \mu \phi^* \right) - |\nabla \phi|^2 - m^2 |\phi|^2. \quad (4)$$

This form is the same as the Euclidean functional integral in the field theory. Thus, we can use the same approach as the zero temperature field theory.

After performing the π integral, the partition function (3) is

$$Z = \int \mathcal{D}\phi \mathcal{D}\phi^* \exp \left\{ \int_0^\beta d\tau \int d^3x \phi^* \times \left[\left(\frac{\partial}{\partial \tau} - \mu \right)^2 + \nabla^2 - m^2 \right] \phi \right\}. \quad (5)$$

Owing to the periodicity $\phi(0, \mathbf{x}) = \phi(\beta, \mathbf{x})$, therefore the Fourier transformation is given by

$$\phi(\tau, \mathbf{x}) = T \sum_{n=-\infty}^{+\infty} \int \frac{d^3 p}{(2\pi)^3} e^{-i(\omega_n \tau - \mathbf{p} \cdot \mathbf{x})} \phi_n(\mathbf{p}), \quad (6)$$

where ω_n is the Matsubara frequency, $\omega_n = 2n\pi T$ ($n = 0, \pm 1, \pm 2, \dots$) for bosons. Using this Fourier transformation, from analogy with zero temperature field theory, the free propagator $D_\beta(i\omega_n, \mathbf{p})$ is given by

$$D_\beta(i\omega_n, \mathbf{p}) = \frac{-1}{(i\omega_n + \mu)^2 - |\mathbf{p}|^2 - m^2}. \quad (7)$$

To distinguish between an imaginary-time Green's function and a real-time Green's function, we refer to $D_\beta(i\omega_n, \mathbf{p})$ as to the thermal Green's function. The thermal Green's function is obtained from the ordinary propagator in the Minkowski space by the replacement,

$$\frac{i}{p^2 - m^2} \Rightarrow \frac{-1}{p^2 - m^2}, \quad p_0 = i\omega_n + \mu. \quad (8)$$

Similarly, the partition function for fermions is given by

$$Z = \int \mathcal{D}\bar{\psi} \mathcal{D}\psi \exp \left\{ \int_0^\beta d\tau \int d^3 x \right. \\ \left. \times \left[\bar{\psi} \left(-\gamma_0 \frac{\partial}{\partial \tau} + i\boldsymbol{\gamma} \cdot \nabla - m + \gamma_0 \mu \right) \psi \right] \right\}. \quad (9)$$

Because a fermion field has the antiperiodicity $\psi(0, \mathbf{x}) = -\psi(\beta, \mathbf{x})$, the Fourier transformation for fermions is

$$\psi(\tau, \mathbf{x}) = T \sum_{n=-\infty}^{+\infty} \int \frac{d^3 p}{(2\pi)^3} e^{-i\omega_n \tau + i\mathbf{p} \cdot \mathbf{x}} \psi_n(\mathbf{p}). \quad (10)$$

The Matsubara frequency for fermions is $\omega_n = 2\pi T(n + 1/2)$ ($n = 0, \pm 1, \pm 2, \dots$). Thus, the free thermal Green's function is given by

$$S_\beta(i\omega_n, \mathbf{p}) = \frac{-1}{(i\omega_n + \mu)\gamma_0 - \boldsymbol{\gamma} \cdot \mathbf{p} - m}. \quad (11)$$

We can use the similar replacement, Eq. (8), for fermions.

III. SCHWINGER-DYSON EQUATION AT NONZERO TEMPERATURE AND CHEMICAL POTENTIAL

The partition function for QED is

$$Z = \int \mathcal{D}A_\mu \mathcal{D}\bar{\psi} \mathcal{D}\psi \exp \left[\int_0^\beta d\tau \int d^3 x \mathcal{L} \right], \quad (12)$$

with

$$\mathcal{L} = \bar{\psi} \left(-\gamma_0 \frac{\partial}{\partial \tau} + \gamma_0 \mu + i\boldsymbol{\gamma} \cdot \nabla - m - e\boldsymbol{A} \right) \psi \\ - \frac{1}{4} F_{\mu\nu} F^{\mu\nu} - \frac{1}{2\xi} (\partial^\mu A_\mu)^2, \quad (13)$$

Here, we used the notation $\partial_\mu = (i\partial/\partial\tau, \nabla)$ and $A_\mu = (A_0, -\mathbf{A})$ in the Minkowski space. Because the argument for QCD is essentially identical to that for QED, we consider

QED for simplicity. Adding sources, the generating functional is given by

$$Z[J_\mu, \eta, \bar{\eta}] = \int \mathcal{D}A_\mu \mathcal{D}\bar{\psi} \mathcal{D}\psi \exp \left[\int_0^\beta d\tau \right. \\ \left. \times \int d^3 x (\mathcal{L} + J_\mu A^\mu + \bar{\eta}\psi + \bar{\psi}\eta) \right]. \quad (14)$$

This form is the same as the Euclidean generating functional apart from the integral range of τ . Thus, using the procedure in the Euclidean (or Minkowski) space [15], the SDE for the fermion thermal Green's function is given by

$$G_\beta^{-1}(p) = -S_\beta^{-1}(p) - e^2 T \sum_l \int \frac{d^3 k}{(2\pi)^3} \gamma_\mu D_\beta^{\mu\nu}(k) \\ \times G_\beta(p-k) \Gamma_\nu(p, k), \quad (15)$$

where G_β is the exact fermion thermal Green's function, $D_\beta^{\mu\nu}$ is the exact photon thermal Green's function, and Γ_ν is the vertex function. $p_0 = i\omega_n + \mu$ is the Matsubara frequency for fermions and $k_0 = i\omega_l$ is the Matsubara frequency for bosons. The free photon thermal Green's function is obtained by the replacement, Eq. (8),

$$\frac{1}{k^2} \left(g^{\mu\nu} + (\xi - 1) \frac{k^\mu k^\nu}{k^2} \right). \quad (16)$$

Because the thermal Green's function has imaginary time or the discrete Matsubara frequency, the thermal Green's function does not correspond to a physical quantity directly. Because of this, it is different from the zero temperature SDE, and the SDE in the imaginary-time formalism should be incomplete to study the chiral phase transition.

To study the chiral phase transition, we use the Cornwall-Jackiw-Tomboulis (CJT) effective potential [16]. The CJT effective potential for QED is given by

$$V[G] = -T \sum_n \text{tr} \int \frac{d^3 p}{(2\pi)^3} \log [G_\beta^{-1}(p) S_\beta(p)] \\ - T \sum_n \text{tr} \int \frac{d^3 p}{(2\pi)^3} S_\beta^{-1}(p) G_\beta(p) + V_2[G], \quad (17)$$

where

$$V_2[G] = \frac{e^2 T^2}{2} \text{tr} \left[\sum_{n,m} \int \frac{d^3 p}{(2\pi)^3} \int \frac{d^3 q}{(2\pi)^3} \gamma_\mu G_\beta(p) \right. \\ \left. \times D_\beta^{\mu\nu}(p-q) \gamma_\nu G_\beta(q) \right]. \quad (18)$$

Here tr indicates a trace over spinor components. We eliminated irrelevant terms.

The exact fermion thermal Green's function can be written as

$$G_\beta(p) = \frac{-1}{C_n(\mathbf{p})\gamma_0 p_0 + A_n(\mathbf{p})\gamma_i p^i - B_n(\mathbf{p})}, \quad (19)$$

where $C_n(\mathbf{p})$, $A_n(\mathbf{p})$, and $B_n(\mathbf{p})$ are arbitrary scalar functions. This is the SO(3) invariant form [7]. At zero temperature, $C(p) = A(p)$ is the wave-function renormalization constant,

and $B(p)$ is the mass function. Inserting Eq. (19) into Eq. (15), the ladder approximation SDEs [6–8,15,17] can be written as

$$C_n(x) = 1 + \frac{e^2 T}{8\pi^2 p_0 x} \sum_m \int_0^\infty dy y \times \frac{-C_m(y)(I_1 + I_2) - A_m(y)I_3}{C_m^2(y)q_0^2 - A_m^2(y)y^2 - B_m^2(y)}, \quad (20)$$

$$A_n(x) = 1 - \frac{e^2 T}{8\pi^2 x^3} \sum_m \int_0^\infty dy y \times \frac{-C_m(y)H_1 + A_m(y)(H_2 - H_3)}{C_m^2(y)q_0^2 - A_m^2(y)y^2 - B_m^2(y)}, \quad (21)$$

$$B_n(x) = -T \frac{3e^2}{8\pi^2 x} \sum_m \int_0^\infty dy \frac{y B_m(y)}{C_m^2(y)q_0^2 - A_m^2(y)y^2 - B_m^2(y)} \times \log \frac{(p_0 - q_0)^2 - (x + y)^2}{(p_0 - q_0)^2 - (x - y)^2}, \quad (22)$$

where $x = |\mathbf{p}|$, $y = |\mathbf{q}|$, p_0 and q_0 are the Matsubara frequency for fermions, and I and H are shown in Appendix A. The fermion is massless, and we adopted the Landau gauge $\xi = 0$. Because $C_n(x)$, $A_n(x)$, and $B_n(x)$ are complex functions, the SDE at nonzero chemical potential is constructed by six simultaneous equations (see Appendix A).

Inserting Eq. (19) into Eqs. (17) and (18), the ladder approximation CJT effective potential is

$$V = -2T \sum_n \int \frac{d^3 p}{(2\pi)^3} \left(\log [-C_n^2(\mathbf{p})p_0^2 + A_n^2(\mathbf{p})|\mathbf{p}|^2 + B_n^2(\mathbf{p})] + \frac{C_n(\mathbf{p})p_0^2 - A_n(\mathbf{p})|\mathbf{p}|^2}{C_n^2(\mathbf{p})p_0^2 - A_n^2(\mathbf{p})|\mathbf{p}|^2 - B_n^2(\mathbf{p})} \right). \quad (23)$$

Because Eqs. (20)–(22) satisfy the relations $C_n(x) = C_{-n-1}^*(x)$, $A_n(x) = A_{-n-1}^*(x)$, and $B_n(x) = B_{-n-1}^*(x)$, using these relations and $\omega_n = -\omega_{-n-1}$ for the fermion Matsubara frequency, one finds that $\text{Im}V$ vanishes. We can see the effect

of the imaginary part of the SDE for the chiral phase transition by using the CJT effective potential.

We do not take into account the Debye screening effect in the gluon thermal Green's function, because this contribution should be unrelated to the imaginary parts. (The Debye screening effect calculated by the hard thermal/dense loop approximation is real [14]).

IV. NUMERICAL CALCULATION

In QCD, the SDEs (20)–(22) replace e^2 with $C_2 g^2$, where C_2 is the Casimir operator. Moreover, the coupling constant g^2 is replaced by a running coupling constant $g^2(-p^2, -q^2)$ (the improved ladder approximation [18]). We adopt the form of a running coupling constant [6,7]:

$$g^2(-p^2, -q^2) = \beta_0 \begin{cases} \frac{1}{t}, & t_F < t, \\ \frac{1}{t_F} + \frac{(t_F - t_C)^2 - (t - t_C)^2}{2t_F^2(t_F - t_C)}, & t_C < t < t_F, \\ \frac{1}{t_F} + \frac{t_F - t_C}{2t_F^2}, & t < t_C, \end{cases} \quad (24)$$

$$t = \log [(-p^2 - q^2)/\Lambda_{\text{qcd}}^2],$$

$$\beta_0 = \frac{48\pi^2}{11N_c - 2N_f}.$$

The parameters are $t_C = -2$, $t_F = 0.5$, $\Lambda_{\text{qcd}} = 592$ MeV, $N_c = 3$, and $N_f = 3$. (Because the value of Λ_{qcd} is not important here, Λ_{qcd} is used as a scale factor.) We assume that strange quark plays a role only in the running coupling and the running coupling has no chemical potential.

The CJT effective potential (23) for QCD is obtained by multiplying by the number of colors $N_c = 3$ and flavors $N_f = 2$. The numbers of colors and flavors result from the trace in Eqs. (17) and (18). To find a critical point for the chiral phase transition, we consider the difference between the Nambu-Goldstone phase [$B_n(x) \neq 0$] and the Wigner phase [$B_n(x) = 0$]. Thus, a critical point is determined by calculating

$$V(B \neq 0) - V(B = 0) = -\frac{N_c N_f T}{\pi^2} \sum_n \int_0^\infty dy y^2 \left\{ \log \left[\frac{-C_n^2(y)p_0^2 + A_n^2(y)y^2 + B_n^2(y)}{-C_n^{W2}(y)p_0^2 + A_n^{W2}(y)y^2} \right] + p_0^2 \left[\frac{C_n(y)}{C_n^2(y)p_0^2 - A_n^2(y)y^2 - B_n^2(y)} - \frac{C_n^W(y)}{C_n^{W2}(y)p_0^2 - A_n^{W2}(y)y^2} \right] - y^2 \left[\frac{A_n(y)}{C_n^2(y)p_0^2 - A_n^2(y)y^2 - B_n^2(y)} - \frac{A_n^W(y)}{C_n^{W2}(y)p_0^2 - A_n^{W2}(y)y^2} \right] \right\}, \quad (25)$$

where C_n^W and A_n^W are solutions at the Wigner phase. If $V(B \neq 0) - V(B = 0) \geq 0$, the chiral symmetry is restored [7]. Because there is a tricritical point at nonzero chemical potential, we especially investigated the effects on tricritical points.

We used the iterative method to solve the SDE. For example, Eq. (22) on the iterative calculation is formally

$$B_{\text{new}}(x) = -T \frac{3e^2}{8\pi^2 x} \sum_m \int_0^\infty dy \frac{y B_{\text{old}}(y)}{C_{\text{old}}^2(y)q_0^2 - A_{\text{old}}^2(y)y^2 - B_{\text{old}}^2(y)} \log \frac{(p_0 - q_0)^2 - (x + y)^2}{(p_0 - q_0)^2 - (x - y)^2}. \quad (26)$$

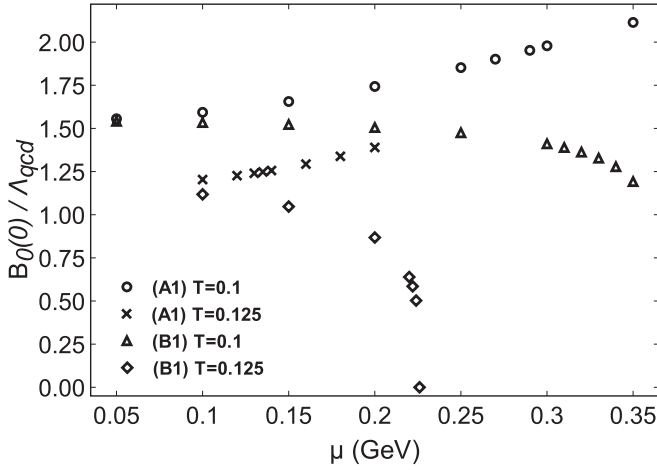


FIG. 1. The chemical potential dependence of $\text{Re}B_0(0)$ in cases (A1) and (B1). To facilitate visualization, we depict the results of $V(B \neq 0) - V(B = 0) \leq 0$.

It repeats until a value is converged. Then, we impose the following restrictions:

- (i) we repeat until a difference between B_{new} and B_{old} becomes of order 10^{-4} MeV, and a difference between C_{new} (A_{new}) and C_{old} (A_{old}) becomes of order 10^{-7} MeV,
- (ii) for a decision on a tricritical point, we consider 10^{-1} MeV order for a temperature and a chemical potential,
- (iii) for a decision on a tricritical point, we consider that a point where $B_n(x)$ has a value of orders of $10^0 \sim 10^{-1}$ MeV before $B_n(x)$ becomes zero numerically is a tricritical point,
- (iv) when $B_n(x)$ has a value of order 10^{-2} MeV, we regard $B_n(x)$ as zero numerically.

We regard $B_n(x)$ as the order parameter for the chiral transition. Thus, the first-order transition $B_n(x)$ becomes zero discontinuously. The second-order transition $B_n(x)$ becomes zero

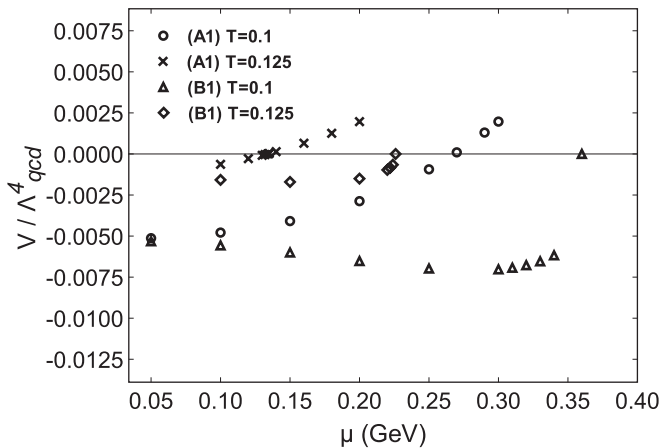


FIG. 2. The chemical potential dependence of $V(B \neq 0) - V(B = 0)$ in cases (A1) and (B1).

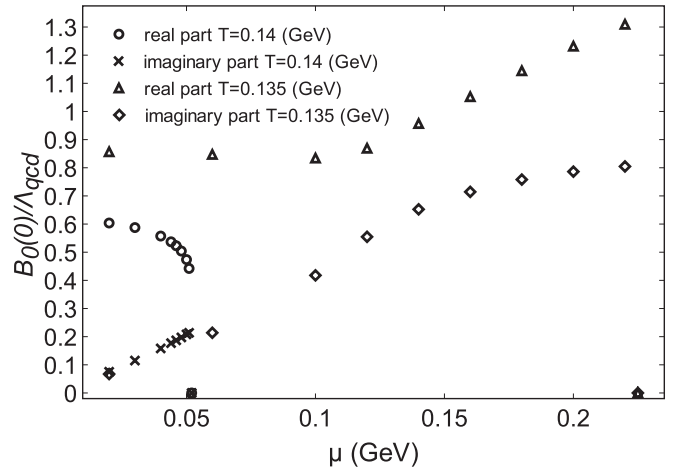


FIG. 3. The chemical potential dependence of $B_0(0)$ in case (A1). $T = 0.135$ and 0.14 GeV.

continuously. Restriction (iii) defines the numerical boundary between the first order and the second order.

A tricritical point fluctuates somewhat by a numerical setup and precision. We note that a tricritical point obtained by our numerical calculation is not highly precise, because our main purpose is to study the effect of an imaginary part. For example, if we take 10^{-2} MeV for the order of $B_n(x)$ in restriction (iii), the tricritical point moves to (142, 35) MeV in case (A1) (see below).

A. Effect of the imaginary part

Since we want to know the effect of the imaginary part of the SDE, we try two cases: (A1) including the imaginary part and (B1) not including the imaginary part. When performing the numerical calculation, we use the real part and the imaginary part of the SDE in case (A1), and we use only the real part of the SDE in case (B1) (fixing $\text{Im}C_n(x)$, $\text{Im}A_n(x)$, and $\text{Im}B_n(x)$ to zero). Then, by inserting a solution in cases (A1) and (B1)

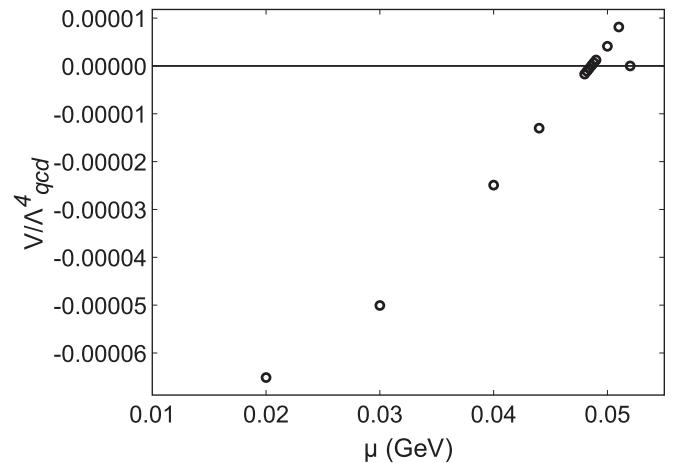


FIG. 4. The chemical potential dependence of $V(B \neq 0) - V(B = 0)$ in case (A1). $T = 0.14$ GeV.

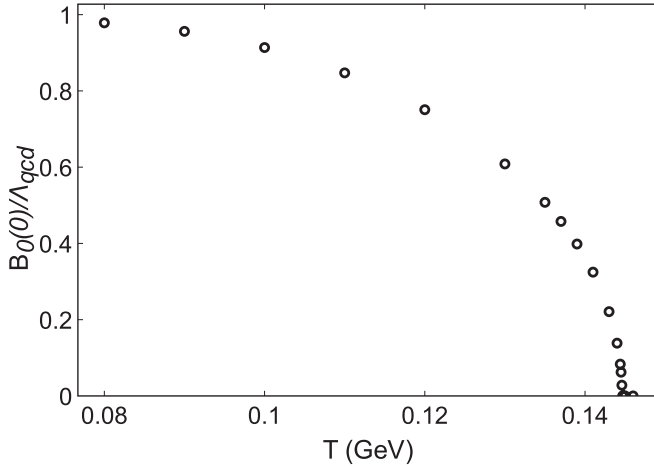


FIG. 5. The temperature dependence of $B_0(0)$ at $\mu = 0$ in case (A1).

into the CJT effective potential, we can verify the effect of an imaginary part for a tricritical point.

The results for cases (A1) and (B1) are shown in Figs. 1 and 2. Figure 1 indicates that the phase transition at nonzero chemical potential is of first order at low temperature (because $B_n(x)$ vanishes discontinuously). The tricritical point in cases (A1) and (B1) are (143, 28) and (128, 209) MeV, respectively (see Fig. 9). $\text{Re}B_0(0)$ and $\text{Im}B_0(0)$ at $T = 0.135$ and 0.14 (GeV) in case (A1) are shown in Fig. 3, and the effective potential at $T = 0.14$ GeV is shown in Fig. 4. Although the process leading to $B_0(0) = 0$ undergoes a change at around the tricritical point, the effective potential is unchanged.

The chemical potential dependence of the effective potential in case (B1) behaves in the same way as the temperature dependence. (The temperature dependence is shown in Figs. 5 and 6.) There is a region where the effective potential $V[B_n(x) \neq 0] - V[B_n(x) = 0]$ does not become positive by increasing the chemical potential. Although $B_n(x)$ decreases smoothly by increasing the chemical potential, $B_n(x)$ vanishes discontinuously. (When nonzero physical quark masses are used, the chiral transition at zero chemical potential becomes

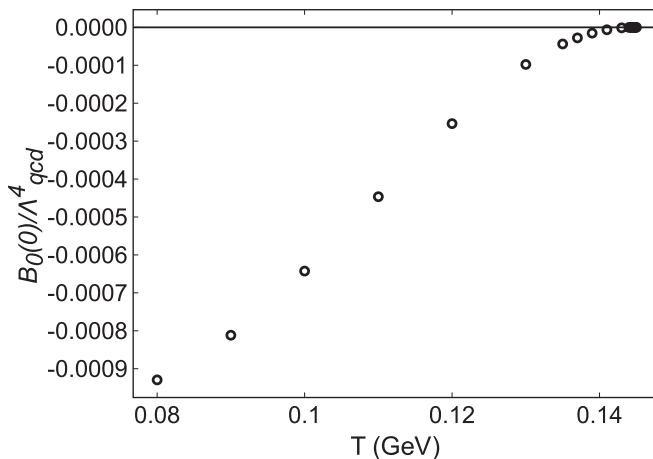


FIG. 6. The temperature dependence of $V(B \neq 0) - V(B = 0)$ at $\mu = 0$ in case (A1).

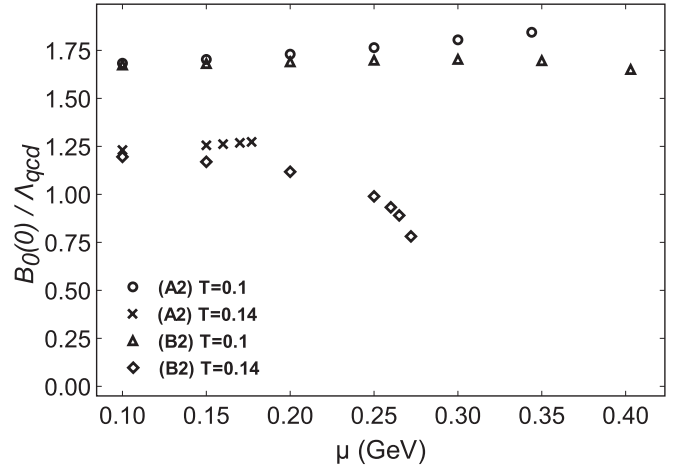


FIG. 7. The chemical potential dependence of $\text{Re}B_0(0)$ in cases (A2) and (B2).

a crossover [19].) Even so, the phase transition is of first order, and a tricritical point exists. In contrast, as mentioned above, although the chemical potential dependence of $B_n(x)$ in case (A1) behaves like the temperature dependence at around the tricritical points, $V[B_n(x) \neq 0] - V[B_n(x) = 0]$ has a positive value.

As a result, the imaginary part affects the phase transition and enhances the effect of the first-order transition. Moreover, the critical chemical potential is displaced by the imaginary part (about 200 MeV).

B. Effect of the wave-function renormalization constant

In place of Eq. (19), we use the exact fermion Green's function,

$$G_\beta(p) = \frac{-1}{\gamma_0 p_0 + \gamma_i p^i - B_n(\mathbf{p})}. \quad (27)$$

This is the approximate form by $C_n(\mathbf{p}) = A_n(\mathbf{p}) = 1$, and this is used from the analogy of zero temperature. (Adopting the Landau gauge, $C(p)$ and $A(p)$ are 1 at zero temperature

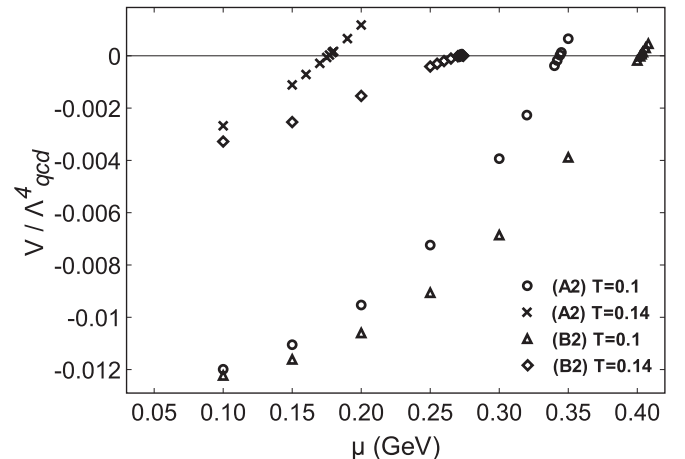


FIG. 8. The chemical potential dependence of $V(B \neq 0) - V(B = 0)$ in cases (A2) and (B2).

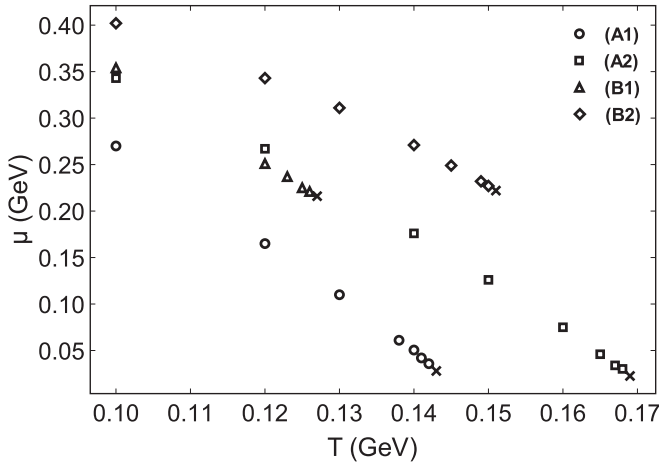


FIG. 9. Tricritical points in cases (A1), (A2), (B1), and (B2). The crosses indicate each tricritical point. The other symbols are the phase transition points of first order.

and chemical potential. However, $C_n(\mathbf{p})$ and $A_n(\mathbf{p})$ are not 1 at nonzero temperature and chemical potential [17].) The effect of the wave-function renormalization constant $C_n(\mathbf{p})$ and $A_n(\mathbf{p})$ is verified by comparing Eqs. (19) and (27). Thus, we calculate two cases:

- (A2) the SDE includes the imaginary part and has no wave-function renormalization constant,
- (B2) the SDE does not include the imaginary part and has no wave-function renormalization constant.

The results obtained using Eq. (27) are shown in Figs. 7 and 8. The chemical potential dependence in cases (A2) and (B2) behaves in the same way as in cases (A1) and (B1). Then, as shown in Fig. 9, the chemical potential at the tricritical point in case (B2) is much larger than that of case (A2): $(T, \mu) = (170, 15)$ MeV in case (A2) and $(151, 222)$ MeV in case (B2). In contrast to this, the temperature of the tricritical point in case (B2) is slightly smaller than that in case (A2). As a result, in case (A1) [(B1)], $C_n(x)$ and $A_n(x)$ decrease the temperature

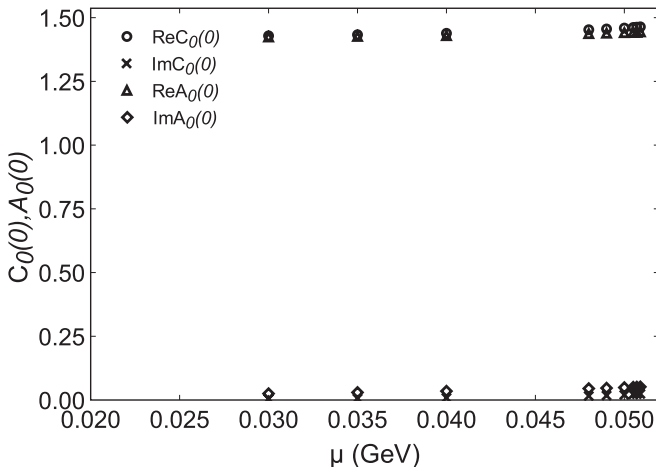


FIG. 10. The chemical potential dependence of $C_0(0)$ and $A_0(0)$. $T = 0.14$ GeV.

of the tricritical point and increase (decrease) the chemical potential of the tricritical point.

The clear effect of the wave function renormalization constant for the tricritical point is to lower the critical temperature. The difference is about 20 MeV. However, because the effect of the wave-function renormalization constant for the critical chemical potential is different in cases (A) and (B), the effect of their imaginary part for the critical chemical potential should be strong. However, Fig. 10 shows that $\text{Im}C_n(x)$ and $\text{Im}A_n(x)$ are very small at around the tricritical point. In contrast, $\text{Im}B_n(x)$ has a value of the same order of $\text{Re}B_n(x)$ at around the tricritical point and has a strong effect [comparing the results of cases (A2) and (B2)]. Thus, the main cause of this difference arises from $B_n(x)$.

V. SUMMARY

In this paper, we calculated the improved ladder approximation SDE at nonzero temperature and chemical potential, and we verified the effect of the imaginary part and the wave-function renormalization constant in the SDE. Considering the imaginary part and the wave-function renormalization constant, all effects in the ladder approximation are included. Thus, we calculated four cases:

- (A1) the SDE includes the imaginary part and has the wave-function renormalization constant,
- (A2) the SDE includes the imaginary part and has no wave-function renormalization constant,
- (B1) the SDE does not include the imaginary part and has the wave-function renormalization constant,
- (B2) the SDE does not include the imaginary part and has no wave-function renormalization constant.

In particular, we took notice of a tricritical point. The tricritical point is $(T, \mu) = (143, 28)$ MeV in case (A1), $(170, 15)$ MeV in case (A2), $(128, 209)$ MeV in case (B1), and $(151, 222)$ MeV in the (B2). The chemical potential at the tricritical point is very small in case (A). This is different from the lattice simulation [20]. There are several reasons for the discrepancy. In particular, the problem is that we do not have the exact information of effective interactions at nonzero chemical potential. If the current lattice simulation at nonzero chemical potential is exact, we must construct an effective interaction that is consistent with the lattice simulation. However, as discussed below, note that $\text{Im}B_n(x)$ affects the tricritical point.

The tricritical point in Ref. [8] is $(142, 82)$ MeV in case (A1) and $(210, 43)$ MeV in case (A2). The difference should result from using a different running coupling constant and a different procedure for the numerical calculation. (From the result in case (A1), although it seems that the temperature at a tricritical point does not depend on a choice of a running coupling constant, it should be a coincidence. So, case (A2) disagrees with our result.) The property that the critical temperature decreases and the critical chemical potential increases when using Eq. (19) in place of Eq. (27) corresponds with our result. Thus, when compared to the critical temperature and the critical chemical potential for $C_n(x) = A_n(x) = 1$

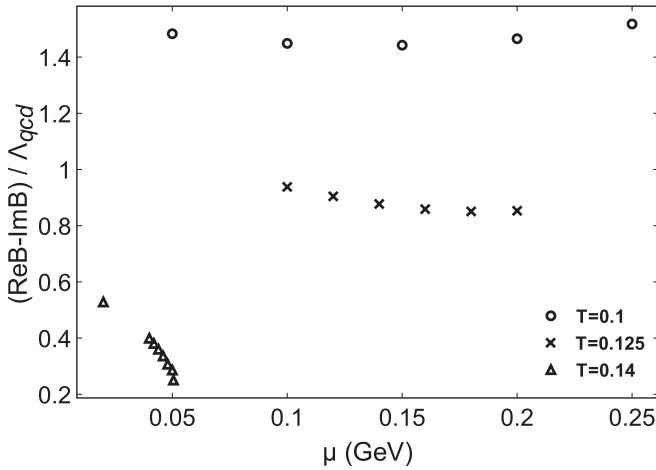


FIG. 11. The difference of $\text{Re}B_0(0)$ and $\text{Im}B_0(0)$. Critical points are (100, 268), (125, 133), and (140, 48) MeV.

at the tricritical point [in cases (A2) and (B2)], the critical temperature decreases and the critical chemical potential increases (decreases) in case (A) [(B)].

Moreover, although a tricritical point is moved by $C_n(x)$ and $A_n(x)$, it is a small move (about 10 MeV). Furthermore, $C_n(x)$ and $A_n(x)$ should not affect the properties of the phase transition strongly. For example, they do not alter the order of the phase transition. Thus, when one studies the chiral phase transition, one should be able to use $C_n(x) = A_n(x) = 1$ sufficiently. (Moreover, their imaginary parts are very small.)

The chemical potential dependence of $B_n(x)$ and the effective potential in case (B) behave like the temperature dependence. When there are not imaginary parts, the effect of temperature, which produces the second-order phase transition, should be stronger. Moreover, the chemical potential of the tricritical point in case (B) is larger than that in case (A) (about 200 MeV). As a result, the imaginary part affects the phase transition and enhances the effect of the first-order transition.

For both cases (A) and (B), the imaginary part moves to the chemical potential largely (above 100 MeV) at the tricritical point. These results for both cases are the same as those in Ref. [9]. In particular, $\text{Im}B_n(x)$ affects a tricritical point strongly. Thus, when one studies a tricritical point, one should not ignore the imaginary part in the SDE. On the other hand, the contribution of $\text{Im}B_n(x)$ is small at a point away from the tricritical point. For example, the critical point is (100, 268) MeV in case (A1) and is (100, 355) MeV in case (B1). This is understood from the fact that the difference between $\text{Re}B_n(x)$ and $\text{Im}B_n(x)$ increases at low temperature (see Fig. 11). Thus, we should be able to ignore the imaginary part at a point away from the tricritical point, because the imaginary part is very small. However, as mentioned above, the chemical potential dependence of the effective potential becomes like the temperature dependence by ignoring the imaginary part. Due to this, although one can ignore the imaginary part in determining a critical point approximately, one should not ignore the imaginary part in studying a property of the phase transition.

Although we considered only the chiral phase transition, there is the deconfinement phase transition in hot and dense QCD. These relations are less well understood. For example, the critical temperature is different in Ref. [21]. However, in Ref. [22], the critical temperature is the same. Moreover, the analysis at nonzero chemical potential is more uncertain. We show the simple result in Appendix B. The behavior of $B_n(x)$ in the chiral limit is identical with that in Ref. [23]. The critical temperature for the chiral phase transition should coincide with the deconfinement transition within the error. However, the critical chemical potential has a gap even in the chiral limit. It is necessary to study the relation between the chiral and the deconfinement phase transition at nonzero chemical potential.

APPENDIX A: I , H , REAL PARTS, AND IMAGINARY PARTS IN THE SDE

We show explicit expressions of I and H in Eqs. (20)–(22):

$$a_+ = (p_0 - q_0)^2 - (x + y)^2, \quad a_- = (p_0 - q_0)^2 - (x - y)^2.$$

- $C_n(x)$

$$I_1 = 2q_0 \log \frac{a_+}{a_-}, \quad I_2 = q_0 \left[-2(p_0 - q_0)^2 \left(\frac{1}{a_+} - \frac{1}{a_-} \right) - \log \frac{a_+}{a_-} \right],$$

$$I_3 = -(p_0 - q_0) \left\{ \log \frac{a_+}{a_-} - [-(p_0 - q_0)^2 + x^2 - y^2] \left(\frac{1}{a_+} - \frac{1}{a_-} \right) \right\}.$$

- $A_n(x)$

$$H_1 = (p_0 - q_0)q_0 \left\{ [x^2 - y^2 + (p_0 - q_0)^2] \left(\frac{1}{a_+} - \frac{1}{a_-} \right) + \log \frac{a_+}{a_-} \right\},$$

$$H_2 = -4xy + [x^2 + y^2 - (p_0 - q_0)^2] \log \frac{a_+}{a_-}, \quad H_3 = \left(x^2 + y^2 - \frac{x^2 + y^2 - (p_0 - q_0)^2}{2} \right) \log \frac{a_+}{a_-} - \left(\frac{(x^2 - y^2)^2 - (p_0 - q_0)^4}{2} \right) \left(\frac{1}{a_+} - \frac{1}{a_-} \right).$$

The real parts and imaginary parts in Eqs. (20)–(22) are

$$\begin{aligned}\text{Re}C_n(x) &= 1 + \frac{e^2 T}{8\pi^3 x} \frac{1}{(\omega_n^2 + \mu^2)} \sum_m \int_0^\infty dy y [(I'_1 + I'_2)(u_1 v_1 - u_2 v_2) + I'_3(v_1 \text{Re}A_m - v_2 \text{Im}A_m)] \frac{1}{R_1^2 + R_2^2}, \\ \text{Im}C_n(x) &= \frac{e^2 T}{8\pi^3 x} \frac{1}{(\omega_n^2 + \mu^2)} \sum_m \int_0^\infty dy y [(I'_1 + I'_2)(u_2 v_1 + u_1 v_2) + I'_3(v_2 \text{Re}A_m + v_1 \text{Im}A_m)] \frac{1}{R_1^2 + R_2^2}, \\ \text{Re}A_n(x) &= 1 + \frac{e^2 T}{8\pi^3 x^3} \sum_m \int_0^\infty dy y [-H'_1(u_1 R_1 + u_2 R_2) + (H_2 - H_3)(R_1 \text{Re}A + R_2 \text{Im}A)] \frac{1}{R_1^2 + R_2^2}, \\ \text{Im}A_n(x) &= \frac{e^2 T}{8\pi^3 x^3} \sum_m \int_0^\infty dy y [-H'_1(u_2 R_1 - u_1 R_2) + (H_2 - H_3)(R_1 \text{Im}A - R_2 \text{Re}A)] \frac{1}{R_1^2 + R_2^2}, \\ \text{Re}B_n(x) &= \frac{3e^2 T}{8\pi^2 x} \sum_m \int_0^\infty dy y \frac{R_1 \text{Re}B_m + R_2 \text{Im}B_m}{R_1^2 + R_2^2} \log \frac{a_+}{a_-}, \quad \text{Im}B_n(x) = \frac{3e^2 T}{8\pi^2 x} \sum_m \int_0^\infty dy y \frac{R_1 \text{Im}B_m - R_2 \text{Re}B_m}{R_1^2 + R_2^2} \log \frac{a_+}{a_-},\end{aligned}$$

where

$$\begin{aligned}R_1 &= (\omega_m^2 - \mu^2)[\text{Re}C_m^2(y) - \text{Im}C_m^2(y)] + 4\mu\omega_m \text{Re}C_m(y)\text{Im}C_m(y) \\ &\quad + y^2[\text{Re}A_m^2(y) - \text{Im}A_m^2(y)] + [\text{Re}B_m^2(y) - \text{Im}B_m^2(y)], \\ R_2 &= 2(\omega_m^2 - \mu^2)\text{Re}C_m(y)\text{Im}C_m(y) - 2\mu\omega_m[\text{Re}C_m^2(y) - \text{Im}C_m^2(y)] \\ &\quad + 2y^2\text{Re}A_m(y)\text{Im}A_m(y) + 2\text{Re}B_m(y)\text{Im}B_m(y), \\ u_1 &= \omega_m \text{Re}C_m(y) + \mu \text{Im}C_m(y), \quad u_2 = \omega_m \text{Im}C_m(y) - \mu \text{Re}C_m(y), \\ v_1 &= \omega_n R_1 + \mu R_2, \quad v_2 = \mu R_1 - \omega_n R_2, \\ I'_1 &= 2 \log \frac{a_+}{a_-}, \quad I'_2 = -2(p_0 - q_0)^2 \left(\frac{1}{a_+} - \frac{1}{a_-} \right) - \log \frac{a_+}{a_-}, \\ I'_3 &= -(\omega_n - \omega_m) \left\{ \log \frac{a_+}{a_-} - [(\omega_n - \omega_m)^2 + x^2 - y^2] \left(\frac{1}{a_+} - \frac{1}{a_-} \right) \right\}, \\ H'_1 &= -(\omega_n - \omega_m) \left\{ [x^2 - y^2 - (\omega_n - \omega_m)^2] \left(\frac{1}{a_+} - \frac{1}{a_-} \right) + \log \frac{a_+}{a_-} \right\}.\end{aligned}$$

APPENDIX B: DECONFINEMENT PHASE TRANSITION

We briefly show a critical point of the deconfinement phase transition at nonzero chemical potential. For this purpose, we use the dual quark condensate as an order parameter for center symmetry. The dual quark condensate is defined by [24]

$$\Sigma_n = \int_0^{2\pi} \frac{d\phi}{2\pi} e^{-i\phi n} \langle \bar{\psi} \psi \rangle_\phi. \quad (\text{B1})$$

Here $\langle \bar{\psi} \psi \rangle_\phi$ is given by

$$\begin{aligned}\langle \bar{\psi} \psi \rangle_\phi &= N_c T \sum_n \int \frac{d^3 p}{(2\pi)^3} \text{tr} G_\beta[\omega_n(\phi), \mathbf{p}] = \frac{2N_c T}{\pi^2} \\ &\quad \times \sum_n \int_0^\infty dx \frac{x^2 B_n(x)}{C_n^2(x)[\omega_n(\phi) - i\mu] + A_n^2(x)x^2 + B_n^2(x)},\end{aligned}$$

where $\omega_n(\phi) = 2\pi T(n + \phi/2\pi)$. $\phi/2\pi$ is caused by the boundary condition $\psi(\beta, \mathbf{x}) = e^{i\phi} \psi(0, \mathbf{x})$. Σ_1 , which is called the dressed Polyakov loop, contains the Polyakov loop. Thus, Σ_{+1} (or Σ_{-1}) is the order parameter for deconfinement.

Although $\langle \bar{\psi} \psi \rangle_{\phi=\pi}$ has no imaginary part, $\langle \bar{\psi} \psi \rangle_{\phi \neq \pi}$ has an imaginary part at nonzero chemical potential. The real

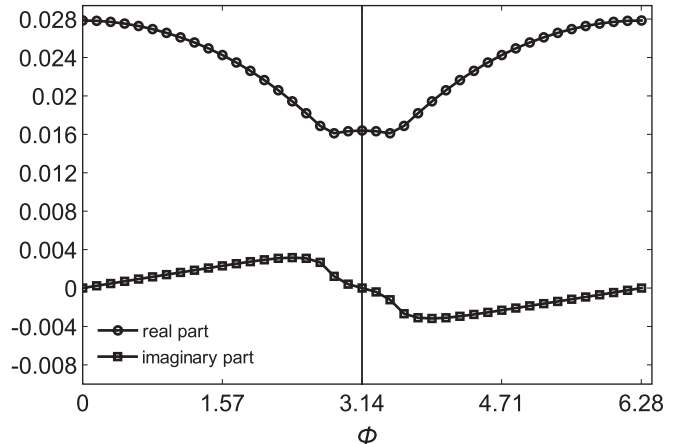


FIG. 12. The angular dependence of $\text{Re}\langle \bar{\psi} \psi \rangle_\phi$ and $\text{Im}\langle \bar{\psi} \psi \rangle_\phi$. $T = 150 \text{ MeV}$. $\mu = 120 \text{ MeV}$.

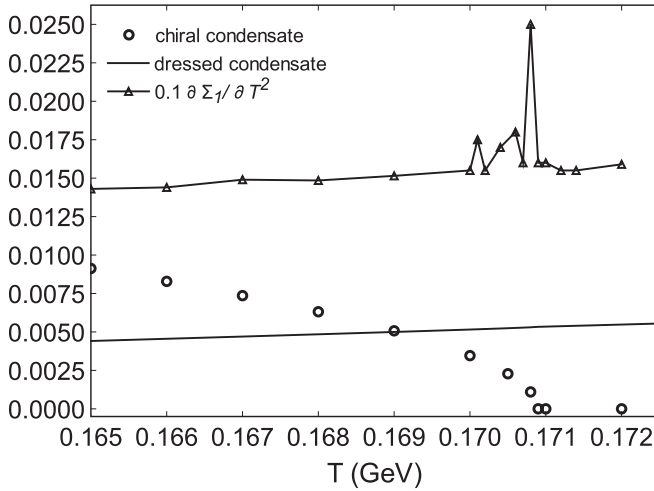


FIG. 13. The temperature dependence of the chiral condensate $\langle \bar{\psi}\psi \rangle_\pi$, the dressed Polyakov loop Σ_1 , and $\partial \Sigma_1 / \partial T$. $\langle \bar{\psi}\psi \rangle_\pi = 0$ indicates the chiral symmetry restoration. $\langle \bar{\psi}\psi \rangle_\pi = 0$ and the peak of $\partial \Sigma_1 / \partial T$ is identical within 1 MeV.

part is symmetric and the imaginary part is antisymmetric (see Fig. 12). For this reason, $\Sigma_{\pm 1}$ becomes

$$\Sigma_{\pm 1} = \int_0^{2\pi} \frac{d\phi}{2\pi} (\text{Re}\langle \bar{\psi}\psi \rangle_\phi \cos \phi \pm \text{Im}\langle \bar{\psi}\psi \rangle_\phi \sin \phi). \quad (\text{B2})$$

The second term vanishes at zero chemical potential.

To find the underlying property, we consider a simple approximation. Thus, we use the ladder approximation, $C_n(x) = A_n(x) = 1$, and the chiral limit [thus, we use Eq. (27)]. The critical temperature for deconfinement can be defined by [23]

$$\tau = \frac{\partial \Sigma_1}{\partial T}. \quad (\text{B3})$$

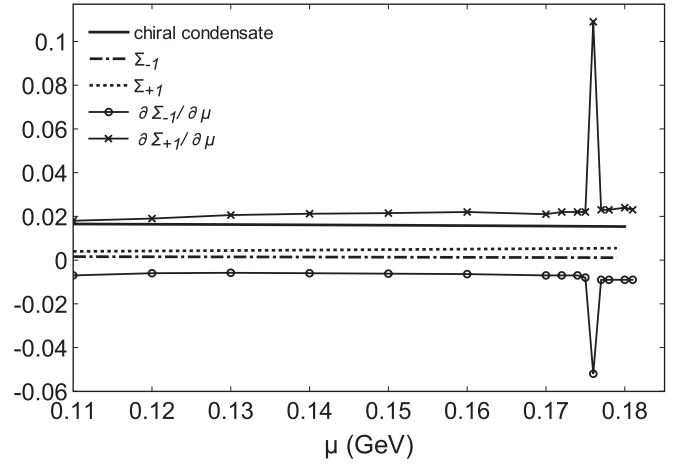


FIG. 14. The chemical potential dependence of the chiral condensate, the dressed Polyakov loop $\Sigma_{\pm 1}$, and $\partial \Sigma_{\pm 1} / \partial \mu$ at $T = 150$ MeV. The critical chemical potential obtained by the effective potential for the chiral phase transition is 127 MeV.

We regard the peak of this as the critical temperature. (τ is not dimensionless.) Similarly, we consider

$$\tau_{\pm} = \frac{\partial \Sigma_{\pm 1}}{\partial \mu}. \quad (\text{B4})$$

Our results are shown in Figs. 13 and 14. The critical temperature for the deconfinement phase transition is identical to that for the chiral phase transition. That is $T = 171$ MeV. This result for the critical temperature in the chiral limit agrees with the result in Ref. [23]. On the other hand, the critical chemical potential is different even in the chiral limit. The difference is about 50 MeV at $T = 150$ MeV. (The critical chemical potential for the chiral phase transition is determined by the effective potential.) Thus, the deconfinement phase transition is clearly distinguished from the chiral transition at nonzero chemical potential.

-
- [1] E. V. Shuryak, *Nucl. Phys. A* **750**, 64 (2005).
[2] M. G. Alford, A. Schmitt, K. Rajagopal, and T. Schäfer, *Rev. Mod. Phys.* **80**, 1455 (2008).
[3] Z. Fodor and S. D. Katz, *Phys. Lett. B* **534**, 87 (2002).
[4] C. R. Allton *et al.*, *Phys. Rev. D* **66**, 074507 (2002).
[5] P. de Forcrand and O. Philipsen, *Nucl. Phys. B* **642**, 290 (2002).
[6] Y. Taniguchi and Y. Yoshida, *Phys. Rev. D* **55**, 2283 (1997).
[7] M. Harada and A. Shibata, *Phys. Rev. D* **59**, 014010 (1998).
[8] T. Ikeda, *Prog. Theor. Phys.* **107**, 403 (2002).
[9] S. Takagi, *Prog. Theor. Phys.* **109**, 233 (2003).
[10] T. Schäfer and F. Wilczek, *Phys. Rev. D* **60**, 114033 (1999).
[11] M. Buballa, *Phys. Rep.* **407**, 205 (2005).
[12] M. Asakawa and K. Yazaki, *Nucl. Phys. A* **504**, 668 (1989); A. Barducci, R. Casalbuoni, S. De Curtis, R. Gatto, and G. Pettini, *Phys. Lett. B* **231**, 463 (1989).
[13] A. L. Fetter and J. D. Walecka, *Quantum Theory of Many-Particle Systems* (McGraw-Hill, New York, 1971).
[14] M. Le Bellac, *Thermal Field Theory* (Cambridge University Press, Cambridge, UK, 1996).
[15] A. Hoell, C. D. Roberts, and S. V. Wright, Lecture Notes Contributed to the Proceedings of the 20th Annual Hampton University Graduate Studies Program (HUGS, 2005), JLab, 31 May–17 June 2005; [arXiv:nuc1-th/0601071v1](https://arxiv.org/abs/nuc1-th/0601071v1).
[16] J. M. Cornwall, R. Jackiw, and E. Tomboulis, *Phys. Rev. D* **10**, 2428 (1974).
[17] S. Sasagawa and H. Tanaka, *Prog. Theor. Phys.* **123**, 533 (2010).
[18] K. Higashijima, *Prog. Theor. Phys. Suppl.* **104**, 1 (1991).
[19] R. V. Gavai and S. Gupta, *Phys. Rev. D* **71**, 114014 (2005).
[20] Y. Nishida, *Phys. Rev. D* **69**, 094501 (2004); X. Q. Luo, *ibid.* **70**, 091504 (2004); N. Kawamoto, K. Miura, A. Ohnishi, and T. Ohnuma, *ibid.* **75**, 014502 (2007).
[21] M. Cheng *et al.*, *Phys. Rev. D* **74**, 054507 (2006).
[22] Y. Aoki *et al.*, *J. High Energy Phys.* **06**(2009)088.
[23] C. S. Fischer and J. A. Mueller, *Phys. Rev. D* **80**, 074029 (2009).
[24] E. Bilgici, F. Bruckmann, C. Gattringer, and C. Hagen, *Phys. Rev. D* **77**, 094007 (2008).